(25)

PPPL-2336

PPPL--2336

DE86 013640

DEGENERATE FOUR-WAVE MIXING AND PHASE CONJUGATION IN A COLLISIONAL PLASMA

By

J.F. Federici and D.K. Mansfield

JUNE 1986

PLASMA PHYSICS LABORATORY

PRINCETON UNIVERSITY

PRINCETON, NEW JERSEY

PREPARED FOR THE U.S. DEPARTMENT OF ENERGY,
UNDER CONTRACT DE-AC02-76-CHO-3073.

PPPL-2336

Degenerate four–wave mixing and phase conjugation in a collisional plasma

J. F. Federici and D. K. Mansfield

Plasma Physics Laboratory, Princeton University

Princeton, NJ 08544

ABSTRACT

Although degenerate four–wave mixing (DFWM) has many practical applications in the visible regime, no successful attempt has been made to study or demonstrate DFWM for wavelengths longer than $10\mu m$. Recently, Steel and Lam established plasma as a viable DFWM and phase conjugation (PC) medium for infrared, far-infrared, and microwaves. However, their analysis is incomplete since collisional effects were not included. Using a fluid description, our results demonstrate that when collisional absorption is small and the collisional mean-free path is shorter than the nonlinear density grating scale length, collisional heating generates a thermal force which substantially enhances the phase conjugate reflectivity. When the collisional attenuation length becomes comparable to the length of the plasma, the dominant effect is collisional absorption of the pump waves. Numerical estimates of the phase conjugate reflectivity indicate that for modest power levels, gains $\gtrsim 1$ are possible in the submillimeter to centimeter wavelength range. This suggests that

a plasma is a viable PC medium at those long wavelengths. In addition, doubly DFWM is discussed.

I. Introduction

Degenerate four–wave mixing (DFWM) and its phase conjugate (PC) properties have received considerable attention in the literature.[1–4] Among their many applications, PC materials have been used in the visible spectrum as cavity resonators and for real time image processing and photolithography. Applications of PC to the infrared and centimeter spectrum include radar imaging and tracking systems and microwave spectroscopy. However, the application of PC techniques to long wavelengths is severely limited since reliable infrared and centimeter PC materials have not yet been realized.

Recently, Steel and Lam[5] proposed that long wavelength PC could be achieved via DFWM using a plasma as the nonlinear medium. From the collisionless two-fluid equations, Steel and Lam calculated that the third order plasma susceptibility ($\chi^{(3)}$) and the reflectivity (R) scale as $\lambda^4 n_e/T_e$ and $\lambda^6 n_e^2/T_e^2$, respectively. Therefore, one is naturally led to seek large reflectivities in cold, dense plasmas. Zhong,[6] who extended the theory to include doubly degenerate four-wave mixing (DDFWM), derived the same scaling as Steel and Lam for $\chi^{(3)}$. Both Steel and Lam and Zhong identified the pondermotive force as the DFWM mechanism. However, for cold, dense plasmas, their analyses are inadequate since collisional effects become important.

In this paper, collisional effects are taken into account using a fluid description. When the collisional attenuation length becomes comparable to the length of the plasma, the expected reflectivity is greatly reduced from the Steel and Lam result due to collisional absorption of the pump waves. However, the third order susceptability may be substantially enhanced above the Steel and Lam result by an additional nonlinear mechanism when collisional absorption is small and the collisional mean-free path is shorter than the nonlinear density grating scale length.

The nonlinear mechanism is the thermal force resulting from localized collisional heating. Numerical estimates of the PC reflectivity indicate that for modest power levels, gains $\gtrsim 1$ are possible in the submillimeter to centimeter wavelength range. In addition, the effect of the sound wave resonance on DDFWM is discussed.

The theory of DFWM and DDFWM in a collisional plasma is presented in Sec. II. Section III contains numerical estimates of the reflectivity. Section IV discusses competing nonlinear effects. Our conclusions are summarized in Sec. V.

II. Theory

In general, the nonlinear polarization of a homogeneous medium may be written as

$$P = \chi^{(1)}E_1 + \chi^{(2)}E_1E_2 + \chi^{(3)}E_1E_2E_3 + \cdots. \tag{1}$$

The $\chi^{(1)}$ term enters the linear dispersion relation. The $\chi^{(3)}$ term represents the coupling of three input waves (two pump waves and a probe wave) to produce the polarization vector of a fourth wave (scattered wave). As long as $\chi^{(3)}$ is nonzero, PC can occur via DFWM. In general, we must consider the $\chi^{(2)}$ term. However, since $\chi^{(2)}$ is only nonzero in a material which lacks inversion symmetry,[7] this term vanishes for an isotropic, unmagnetized plasma.

Physically, DFWM and DDFWM can be explained in terms of one of the pump waves scattering from a density modulation. The density modulation is formed when one of the pump waves and the probe couple via some nonlinear microscopic process to form a low frequency density grating in space

$$n_2^s \sim \exp[i(\mathbf{k}_m - \mathbf{k}_p)\cdot\mathbf{r} - i(\omega_m - \omega_p)t],$$

where p refers to the probe and m refers to either of the pumps (Fig. 1). The high frequency contribution $\omega_m + \omega_p$ has negligible effect on $\chi^{(3)}$. The other pump wave

scatters from the grating to produce the scattered signal wave. Likewise, one could consider the probe wave coupling to the other pump wave. In order to produce the PC partner of the probe wave rather than some arbitrary fourth wave, the following phase matching conditions must be satisfied in DFWM:

$$\mathbf{k}_s = \mathbf{k}_f + \mathbf{k}_b - \mathbf{k}_p \qquad \omega_s = \omega_f + \omega_b - \omega_p. \tag{2}$$

In the above expression, the foward pump, backward pump, probe, and scattered wave are denoted by f,b,p,s as in Fig. 1. For DFWM, the frequency phase matching condition is trivially satisfied since all of the frequencies are identical. If the pump beams are antiparallel, then $\mathbf{k}_f + \mathbf{k}_b = 0$, $\mathbf{k}_s = -\mathbf{k}_p$, and a phase conjugate signal of the probe can be produced. For DDFWM the phase matching conditions are

$$\mathbf{k}_s = \mathbf{k}_f + \mathbf{k}_b - \mathbf{k}_p \qquad \omega_s - \omega_f = 0 \quad \omega_b - \omega_p = 0. \tag{3}$$

In DDFWM the frequency conditions are satisfied since the foward pump and scattered wave frequencies differ from the backward pump and probe frequencies. The wave vector matching condition determines the relative angles among the pump, probe, and signal wave vectors. By appropriate orientation of the waves, it is possible to use DDFWM as a real time image conversion process.[8]

DWFM in a plasma was first studied by Steel and Lam.[5] Using the collisionless fluid equations, they identified the pondermotive force

$$\mathbf{F} = \frac{-q^2}{2m\omega^2}\nabla\langle E_o^2\rangle$$

as the microscopic mechanism which generates the density modulation in the plasma. When two waves couple together in the plasma, the pondermotive force pushes particles into regions of low $\mid E \mid$ to form a density grating. Another wave scatters from the density grating to produce the PC wave. Steel and Lam calculated $\chi^{(3)}$ to be

$$\chi^{(3)} = \frac{n_e/N_c^2}{(4\pi)^2[T_e + T_i/(1+\mid \mathbf{k}_m - \mathbf{k}_p \mid^2 \lambda_{di}^2)]} \tag{4}$$

which scales as $\chi^{(3)} \sim \lambda^4 n_e/T_e$. Here $N_c = m_e\omega^2/4\pi e^2$ is the critical density at the pump frequency ω.

For $k\lambda_{mfp} \ll 1$, Eq. (4) is incorrect since collisional effects become important. In order to include collisional contributions to $\chi^{(3)}$, our corrections to Steel and Lam involve two sets of equations for the two distinct time scales. In the DFWM analysis there is the fast pump time scale which is described by fluid equations with only collisional damping included and the low frequency density modulation time scale which is described by collisional fluid equations. The wave vector and frequency of the pump time scale fluctuations are $\mathbf{k}_n$ and ω_n where n refers to the pump, probe, or scattered waves. The slow time scale wave vector and frequency are denoted by

$$\mathbf{k}_{mn} = \mathbf{k}_m - \mathbf{k}_n^* \qquad \omega_{mn} = \omega_m - \omega_n,$$

where m and n refer to the pumps or probe.

The fluid equations governing the fast oscillations are

$$\frac{\partial N}{\partial t} + \nabla \cdot (N\mathbf{V}) = 0, \tag{5}$$

$$\frac{d\mathbf{V}}{dt} = -\frac{\nabla P}{mN} + \frac{q}{m}(\mathbf{E} + \frac{1}{c}\mathbf{V} \times \mathbf{B}) \pm \frac{\mathbf{F}}{mN}, \tag{6}$$

where $\mathbf{F}$ is the collisional drag term. This term is negligible in the ion equation. For the electron equation

$$\mathbf{F} = m_e N_o \nu_{hf}(\mathbf{v}_e - \mathbf{v}_i), \tag{7}$$

$$\nu_{hf} = \frac{\nu_e}{2}\left(1 + \frac{\ln(\sqrt{2}\frac{\omega_{pe}}{\omega}) - \frac{\gamma}{2}}{\ln\Lambda}\right), \tag{8}$$

where ν_{hf} is the high frequency collision rate and ν_e is the fluid electron-ion collision frequency. The high frequency collision rate and absorption coefficient are derived in Appendix A.

The low frequency oscillations evolve according to collisional fluid equations for singly charged ions and $\mathbf{B_o} = 0$.[9] Viscous effects are small and have been neglected. Likewise, the intensity of the pump waves is assumed to be small enough that the contributions from the high frequency field to the plasma transport may be neglected.

The low frequency fluid equations are

$$\frac{\partial N}{\partial t} + \nabla \cdot (N\mathbf{V}) = 0, \tag{9}$$

$$\frac{d\mathbf{V}}{dt} = -\frac{\nabla P}{mN} + \frac{q}{m}(\mathbf{E} + \frac{1}{c}\mathbf{V} \times \mathbf{B}) \pm \frac{\mathbf{R}}{mN}, \tag{10}$$

$$\frac{3}{2}N\frac{dT}{dt} + P\nabla \cdot \mathbf{V} = -\nabla \cdot \mathbf{q} + Q_{coll}, \tag{11}$$

where $N, \mathbf{V}, p$, and T are the fluid density, velocity, pressure and temperature, respectively. $\mathbf{E}, \mathbf{B}, \mathbf{R}, \mathbf{q}$, and Q_{coll} are the electric field, magnetic field, collisional momentum transfer, heat flux, and collisional heating, respectively.

Equations (5) to (11) are solved using a perturbative expansion for density, velocity, electric field, etc. in powers of the pump electric field. All first order terms oscillate on the fast time scale while the second order terms evolve on the slow time scale:

$$\begin{aligned} N &= N_o + n_1(k_n, \omega_n) + n_2(k_{mn}, \omega_{mn}), \\ V &= 0 + V_1(k_n, \omega_n) + V_2(k_{mn}, \omega_{mn}), \\ E &= 0 + E_1(k_n, \omega_n) + E_2(k_{mn}, \omega_{mn}), \\ T &= T_o + T_1(k_n, \omega_n) + T_2(k_{mn}, \omega_{mn}). \end{aligned} \tag{12}$$

In the expansion, $k_{mn}\lambda_{di}, k_{mn}\lambda_{mfp}$, and ν_e/ω_n (or equivalently $\lambda_n v_{te}/\lambda_{mfp}c$) are assumed small. E_1 is the imposed laser beam electric field and E_2 is the self-consistent plasma electric field. The equilibrium density and temperature are constant. The probe, pump, and signal electric fields are approximated as plane waves

$$\mathbf{E}_1 = \frac{1}{2}\Big(\mathbf{E}_{1n}\exp[i\mathbf{k}_n \cdot \mathbf{r} - i\omega_n t] + \mathbf{E}_{1n}^*\exp[-i\mathbf{k}_n^* \cdot \mathbf{r} + i\omega_n t]\Big), \tag{13}$$

where $\mathbf{k}_n = \mathbf{k}_{r_n} + i\alpha\hat{\mathbf{k}}_{r_n}$, α is the absorption coefficient which is derived in Appendix A, ω_n is the wave frequency (positive definite), $\mathbf{k}_n$ is the wave vector (choosing $\mathbf{k}$ defines direction of propagation), and n refers to the foward pump, backward pump , or the probe wave. Furthermore, we assume that the input waves propagate as ordinary waves.

The validity of the plane wave approximation requires that the laser pulse must be long compared to the typical formation time of the density modulation $n_2(k_{mn}, \omega_{mn})$. The formation time is determined by the sound frequency

$$\tau_{form} \sim \frac{1}{k_{mn} c_s}.$$

Our objective is to calculate the third order $\chi^{(3)}$ using the third order perturbed current. The major contribution to $\mathbf{J}_3$ takes the form

$$\mathbf{J}_{3s} \simeq -\frac{1}{2} e n^e_{2mn} \mathbf{v}^e_{1l}, \tag{14}$$

where n^e_{2mn} is the low frequency density grating (slow time scale) and $\mathbf{v}^e_{1l}$ is the first order perturbed velocity (pump frequency fast time scale). The collisional fluid equations are valid in calculating n^e_{2mn} since the collision frequency is assumed to be larger than the grating frequency and the mean-free path is shorter than the grating scale length $1/k_{mn}$.

Proceeding with the calculation of $\chi^{(3)}$, Eqs. (5) to (6) yield to first order $n^e_1 = n^i_1 = T^e_1 = T^i_1 = 0$ and

$$\mathbf{v}^e_1 = -\frac{1}{2} \frac{ie\mathbf{E}_{1m}}{m_e \omega} \exp[i\mathbf{k}_m \cdot \mathbf{r} - i\omega_m t] + c.c., \tag{15}$$

since $\mathbf{k} \cdot \mathbf{E}_1 = 0$.

When Eqs. (9) to (11) are solved for the second order slow time scale terms using the expansion given by Eq. (12), coupling terms such as $\mathbf{v}_1 \times \mathbf{B}_1$ have the

form

$$\exp[i\mathbf{k}_{mn}\cdot\mathbf{r}-i\omega_{mn}t]\sum_{m,n}(\mathbf{v}_{1m}\times\mathbf{B}_{1n}^{*})+\text{c.c.}\ .$$

The coupling terms represent the nonlinear processes which generate the density modulation. Using Eqs. (12), (9), and (10), the second order electron and ion density fluctuations are

$$n_2^e = \frac{1}{2}n_{2mn}^e\exp[i\mathbf{k}_{mn}\cdot\mathbf{r}-i\omega_{mn}t]+\text{c.c.}, \tag{16}$$

$$n_{2mn}^e = \frac{-1.71k_{mn}^2T_{2mn}^eN_o/m_e+n_{2mn}^i(\omega_{pe}^2-i.51\omega_{mn}\nu_e)}{k_{mn}^2v_{te}^2-\omega_{mn}^2+\omega_{pe}^2-i.51\omega_{mn}\nu_e}$$

$$-\frac{k_{mn}^2N_o(\mathbf{v}_{1m}^e\cdot\mathbf{v}_{1n}^{e*})/4}{k_{mn}^2v_{te}^2-\omega_{mn}^2+\omega_{pe}^2-i.51\omega_{mn}\nu_e}, \tag{17}$$

$$n_2^i = \frac{1}{2}n_{2mn}^i\exp[i\mathbf{k}_{mn}\cdot\mathbf{r}-i\omega_{mn}t]+\text{c.c.}, \tag{18}$$

$$n_{2mn}^i = \frac{-k_{mn}^2T_{2mn}^iN_o/m_i+.71k_{mn}^2T_{2mn}^eN_o/m_i+n_{2mn}^e(\omega_{pi}^2-i.51\omega_{mn}\nu_e)}{\omega_{pi}^2-\omega_{mn}^2-i.51\omega_{mn}\nu_e}. \tag{19}$$

The last term in Eq. (17) results from combining the Lorentz term $\mathbf{v}_1\times\mathbf{B}_1$ and the convective term $\mathbf{v}_1\cdot\nabla\mathbf{v}_1$ to form the familiar pondermotive term $\frac{1}{2}\nabla(\mathbf{v}_1\cdot\mathbf{v}_1)$.

Similarly, using Eqs. (11) and (12), the temperature fluctuations are

$$T_2^e = \frac{1}{2}T_{2mn}^e\exp[i\mathbf{k}_{mn}\cdot\mathbf{r}-i\omega_{mn}t]+\text{c.c.}, \tag{20}$$

$$T_{2mn}^e = \frac{-1.71iT_e\omega_{mn}n_{2mn}^e+.71iT_e\omega_{mn}n_{2mn}^i+3\frac{m_e}{m_i}N_o\nu_eT_{2mn}^i}{\kappa^ek_{mn}^2+3\frac{m_e}{m_i}N_o\nu_e-i\frac{3}{2}\omega_{mn}N_o}$$

$$+\frac{.51N_om_e\nu_e\mathbf{v}_{1m}^e\cdot\mathbf{v}_{1n}^{e*}/2}{\kappa^ek_{mn}^2+3\frac{m_e}{m_i}N_o\nu_e-i\frac{3}{2}\omega_{mn}N_o}, \tag{21}$$

$$T_2^i = \frac{1}{2}T_{2mn}^i\exp[i\mathbf{k}_{mn}\cdot\mathbf{r}-i\omega_{mn}t]+\text{c.c.}, \tag{22}$$

$$T_{2mn}^i = \frac{3\frac{m_e}{m_i}N_o\nu_eT_{2mn}^e-iT_i\omega_{mn}n_{2mn}^i}{k_{mn}^2\kappa^i+3\frac{m_e}{m_i}N_o\nu_e-i\frac{3}{2}\omega_{mn}N_o}. \tag{23}$$

In the above equations, $\kappa^e(\kappa^i)$ is the electron (ion) thermal conductivity. In solving for $\chi^{(3)}$, two cases are considered: $\omega_{mn} \sim 0$ (DFWM) and $\omega_{mn} \sim k_{mn}c_s$. For the second case, the sound waves which are excited enhance n^e_{2mn}, $\chi^{(3)}$, and the reflectivity.

The DFWM $\chi^{(3)}$ is derived using Eqs. (14) to (23) and $\omega_{mn} \to 0$. The third order current density is

$$\mathbf{J}_3 = \frac{1}{2}\mathbf{J}_{3s}\exp[i(\mathbf{k}_l + \mathbf{k}_m - \mathbf{k}^*_n)\cdot\mathbf{r} - i\omega_l t] + \text{c.c.}, \tag{24}$$

$$\mathbf{J}_{3s} = \frac{-ie^4 N_o \mathbf{E}_{1l}}{8m_e^2\omega_m\omega_n\omega_l[T_e + T_i]}\Big[(\mathbf{E}_{1m}\cdot\mathbf{E}^*_{1n}) + [1 + \frac{3m_e/m_iN_o\nu_e}{(\kappa^i k^2_{mn} + 3m_e/m_iN_o\nu_e)}]\frac{1.02N_o\nu_e}{\kappa^e k^2_{mn}}(\mathbf{E}_{1m}\cdot\mathbf{E}^*_{1n})\Big]. \tag{25}$$

In the above calculation, the ion velocity is neglected compared to the electron velocity. It is apparent from the phase matching conditions, Eq. (2), that n must refer to the probe and l and m refer to either of the pumps.

Writing $\mathbf{P}_s = \frac{1}{2}\chi^{(3)}_{ml}(\mathbf{E}_{1m}\cdot\mathbf{E}^*_{1p})\mathbf{E}_{1l}\exp[i\mathbf{k}_s\cdot\mathbf{r} - i\omega_s t] + \text{c.c.}$, one can use Eq. (25) to derive

$$\chi^{(3)}_{ml} = \frac{N_o/N_e(\omega_m)N_e(\omega_p)}{8(4\pi)^2(T_e + T_i)}\Big[1 + [1 + \frac{3m_e/m_iN_o\nu_e}{(\kappa^i k^2_{mn} + 3m_e/m_iN_o\nu_e)}]\frac{1.02N_o\nu_e}{\kappa^e k^2_{mn}}\Big]. \tag{26}$$

If collisions are ignored, Eq. (26) reduces to Zhong's result. Furthermore, setting $\omega_m = \omega_p$ reproduces Steel and Lam's expression for $\chi^{(3)}$.

The collisional contribution to $\chi^{(3)}$ is produced by local plasma heating balancing the thermal conduction of electrons

$$\kappa^e\nabla^2 T_e \sim -m_e N_o\nu_e(\mathbf{v}^e_{1m}\cdot\mathbf{v}^{e*}_{1n}).$$

The pressure gradient due to collisional heating pushes the electrons into regions of minimum $|E|$ thereby supplementing the pondermotive force. This is identical to the microscopic thermal force which leads to thermally enhanced self-focusing.[13]

One of the attractive characteristics of DDFWM is the prospect of enhancing the $\chi^{(3)}$ and PC reflectivity by matching the frequency difference between the probe and one of the pumps to a plasma resonance. In a collisional unmagnetized plasma, a potential resonance exists near $\omega_{mn}^2 \simeq k_{mn}^2 c_s^2$ where c_s is the sound speed. The sound wave resonance may be studied with our model as long as $\omega_{mn} < \nu_e$. The difference frequency must satisfy the relation

$$\omega_{mn} = \mid \omega_m - \omega_n \mid = \mid \mathbf{k}_m - \mathbf{k}_n \mid c_s.$$

In order to simplify the analytic calculation, additional orderings are assumed. Since $\chi^{(3)}$ is expected to reach a maximum near cutoff, we choose orderings which are valid in this regime. At high densities close to cutoff, $\omega_{mn}\nu_e/\omega_{pi}^2 \ll 1$ and $\nu_e m_e/\omega_{mn} m_i \ll 1$. Under these restrictions

$$\chi_{ml}^{(3)} = \frac{N_o/N_c(\omega_m)N_c(\omega_p)}{8(4\pi)^2 T_e(1-D_o)}\left[1+\frac{1.02N_o\nu_e}{\kappa^e k_{mn}^2}\right], \tag{27}$$

$$D_o = \frac{\omega_{mn}^2}{k_{mn}^2 c_s^2}\left[1+i\left(\frac{.51\nu_e\omega_{mn}}{\omega_{pi}^2}+\frac{4k_{mn}^2 v_{ti}^2}{9\omega_{mn}^2}\frac{k_{mn}^2\kappa^i+3\frac{m_e}{m_i}\nu_e N_o}{\omega_{mn}N_o}+\frac{k_{mn}c_s}{\omega_{mn}}\frac{k_{mn}c_s N_o}{k_{mn}^2\kappa^e}\right)\right].$$

The real portion of the denominator $(1-D_o)$ vanishes when $\omega_{mn}^2 \simeq k_{mn}^2 c_s^2$. By the above orderings, the sound wave is weakly damped since the imaginary portion of the denominator is much less than the real part. Therefore, $\chi_{ml}^{(3)}$ and the PC reflectivity should exhibit a resonance at the sound wave frequency.

III. Numerical Results

Once $\chi^{(3)}$ is known from plasma theory, the expected phase conjugate reflectivity may be calculated assuming a simplified experimental configuration. For the DFWM case, we assume that all of the input waves are (nearly) collinear and have the same planar polarization. For the collinear case, the coupling of the probe wave

to the two different pump waves produces two distinct density modulation scale lengths. The coupling of the backward pump and probe generate a modulation with scale length $1/k_{bp} \sim 1/2k_b$. The forward pump and probe generate a density modulation whose scale length becomes very large ($1/k_{fp} \sim 1/(k_f - k_p)$). Since $k_{fp}L \ll 1$ for collinear propagation where L is the DFWM interaction length, this contribution to $\chi^{(3)}$ is negligible. Under these assumptions, Eq. (26) becomes

$$\chi^{(3)} = \frac{N_o/N_c(\omega_b)N_c(\omega_p)}{8(4\pi)^2(T_e+T_i)}\Big[1+[1+\frac{3m_e/m_iN_o\nu_e}{\kappa^i k_{mn}^2+3m_e/m_iN_o\nu_e}]\frac{1.02N_o\nu_e}{\kappa^e k_{bp}}\Big], \quad (28)$$

where m and n are explicitly replaced by b and p, respectively. The dominant pondermotive and thermal terms in the above expression are

$$\chi^{(3)} \sim \frac{N_o/N_c(\omega_b)N_c(\omega_p)}{8(4\pi)^2(T_e+T_i)}\Big[1+\frac{1.02N_o\nu_e}{k_{bp}^2\kappa^e}\Big]. \quad (29)$$

Physically, the second term in brackets arises from the thermal force due to localized collisional heating. Using Eq. (29) and the definition of κ^e, the criterion for significant thermally enhanced DFWM is $\lambda_{mn}/\lambda_{mfp} > 1$.

Given $\chi^{(3)}$ and α, the expected reflected power is given by[11]

$$R = \frac{4\kappa^2\tan^2(\kappa_e L)e^{-2\alpha L}}{|\,2\alpha\tan(\kappa_e L)+2\kappa_e\,|^2}, \quad (30)$$

$$\kappa_e = (\kappa^2 e^{-2\alpha L}-\alpha^2)^{\frac{1}{2}}, \quad (31)$$

$$\kappa = |\,\frac{2\pi\omega_b}{cn_o}\chi^{(3)}E_f E_b\,|, \quad (32)$$

where n_o is the index of refraction and L is the interaction length. Note that $R \not< 1$. In particular, when the denominator nearly vanishes, one would expect large gain.

Using Eq. (28) and Eqs. (30) to (32), the expected reflectivity can be calculated for a variety of plasma and wave sources. For simplicity, the plasma is assumed to be singly charged argon. Figure 2 shows the result for a CW CO_2 laser with an intensity of 2×10^5 W/cm^2. The dashed line is Steel and Lam's result. The limit

of validity of the fluid equations $k_{mn}\lambda_{mfp} \sim 1$ is near $n_e \sim 4 \times 10^{16}\ cm^{-3}$ when $T_e \sim 0.75\ eV$. At low density, collisions become unimportant. Thus our results approach Steel and Lam. At very high density, the dominant effect is the spatial attenuation of the input waves by collisional damping. At moderate densities, the reflectivity is enhanced by the thermal force. As T_e increases, the thermal force becomes less important than the pondermotive force. For $n_e \sim 10^{17}$ and $T_e \gg T_i$, $\chi^{(3)}$ and the reflectivity scale as

$$\chi^{(3)} \sim \frac{N_o/N_c^2}{15700T_e}\frac{1}{k_n^2\lambda_{mfp}^2},$$

$$R \sim \left(\frac{1}{200}\frac{\omega_n L}{c}\frac{N_o}{N_c}\frac{1}{k_n^2\lambda_{mfp}^2}\left(\frac{E_n^2e^2}{m_e\omega_n^2}/T_e\right)\right)^2.$$

Since the reflectivity scales as the square of the intensity, one would expect greatly enhanced reflectivity for a pulsed CO_2 laser. For an intensity of 150 MW/cm^2, the reflectivity approaches 1 (Fig. 3). As before, collisional effects enhance the reflectivity above the Steel and Lam result for $k_{mn}\lambda_{mfp} \ll 1$ and negligible collisional damping.

At longer wavelengths, lower intensities are required since the reflectivity scales like λ^{10}. At far-infrared wavelengths, modest intensities on the order of $2.5 MW/cm^2$ produce reflectivities on the order of 1 due to thermally enhanced DFWM (Fig. 4). Likewise, for 2 mm waves (Fig. 5), reflectivities of order unity are expected near cutoff. For 1 cm waves, the fluid equations are invalid since $k_{mn}\lambda_{mfp} \sim 1$ for $T_e \sim 1\ eV$ near cutoff. However, Steel and Lam's theory should provide a reasonable estimate of the reflectivity (Fig. 6).

Reflectivity resulting from DDFWM is calculated in an analogous fashion to DFWM. Since we are interested in maximizing the PC reflectivity, we take $\omega_{mn} = k_{mn}c_s$ in Eq. (27). Fig. 7 shows the expected results for a CW CO_2 laser with intensity $2 \times 10^5\ W/cm^2$. The dashed line indicates what the result would have been

if $D_e = 0$. The difference between the curves represents the enhanced reflectivity resulting from the sound wave resonance. Similar results are obtained for far-infrared and millimeter wavelengths (Figs. 8 and 9). The enhancement for the 2 mm waves is particularly striking.

IV. Competing Effects

Although the scaling laws presented in the previous sections suggest that gains of order one might be achieved by simply employing intense pump beams, numerous competing effects such as self-focusing,[12,13] Stimulated Brillouin Scattering (SBS), and Stimulated Raman Scattering[14,15] (SRS) could potentially limit the pump intensities or dominate the DFWM phenomenon. However, as Steel and Lam have shown, pondermotive self-focusing, SBS, and SRS are negligible in many plasmas of interest to DFWM. These effects are small since they generally require large threshold powers or long interaction lengths. Unlike SRS, SBS, and self-focusing, there is no threshold power for DFWM. In addition, for many plasmas of interest the optimal interaction length in DFWM is much shorter than typical gain scale lengths ($k_i L \ll 1$) for SBS, SRS, and self-focusing instabilities. For the collisional plasmas discussed in Sec. III, the optimal interaction length for DFWM is limited by collisional damping.

In addition to the competing effects discussed by Steel and Lam, thermal self-focusing must be considered in collisional plasmas. The onset of thermal self-focusing is characterized by three threshold conditions. The power of the laser beam must exceed the threshold

$$P_T \simeq 5.2 \times 10^{21} \frac{n_{cr}}{n_e} \frac{T_e^2}{a^2 \nu_e^2} \quad W. \tag{33}$$

The interaction length threshold is defined by the condition that the intensity of

the focusing beam exponentiated once in a plasma of length L $(2k_iL = 1)$. The collisional damping threshold is estimated by $2k_i/\alpha = 1$ where α is the absorption coefficient. The interaction length and collisional damping thresholds for thermal self-focusing are[13]

$$I_{Tl} \simeq 2 \times 10^4 (\frac{n_{cr}}{n_e})^3 (\frac{\lambda}{L})^2 T_e^5 \quad W/cm^2, \tag{34}$$

$$I_{Tc} \simeq .6 \frac{n_e}{n_{cr}} \frac{T_e^2}{\lambda^2} \quad W/cm^2, \tag{35}$$

where T_e is the electron temperature in eV, n_{cr} is the critical density at the laser frequency, n_e is the electron density, λ is the laser wavelength, L is the typical length of the plasma, and a is the spot size of the laser beam. For $T_e = 1\ eV, n_e = 2 \times 10^{17}, \lambda = 10\ \mu m, a = 0.05\ cm$ and $L = 5\ cm$, the power threshold is $P_T \simeq 36\ W$, while the other thresholds are $I_{Tl} \simeq 140\ W/cm^2$ and $I_{Tc} \simeq 11\ kW/cm^2$. These small thresholds may be easily exceeded, for example, using a CO_2 laser in 5 cm long plasma.

A qualitative picture of self-focusing may be used to assess the effect of this focusing on DFWM. If the pump and probe waves propagate as Gaussian beams, the beams suffer whole-beam self-focusing. This effect is largely benevolent to DFWM since the PC reflectivity should increase with beam intensity. However, as the beams focus, particles are pushed out of the path of the propagating beam by the thermal force thereby reducing the plasma density in the DFWM interaction region and potentially degrading the PC reflectivity. One simple measure of the limiting power beyond which thermal self-focusing leads to significant reduction of electron density in the interaction region is obtained by requiring the thermally focused beam to reduce the density by 1/e. This limiting power P_l may be calculated using the expression for the intensity-dependent electron density.[13] Following the

formalism of Ref. 13, we write

$$n_e = n_o e^{-e\phi_t/T_e},$$

$$e\phi_t = \frac{8\alpha I a^2}{\pi^2 \kappa^e},$$

where ϕ_t is the thermal potential, α is the attenuation coefficient, κ^e is the electron thermal conduction, I is the intensity, and a is the typical spot size of the beam. Setting $e\phi = T_e$ defines the limiting power

$$P_l = \frac{\pi^3 T_e \kappa^e}{8\alpha}. \tag{36}$$

For $T_e = 1\ eV, n_e = 2 \times 10^{17}$,and$\lambda_{mn} = 10\ \mu m$, the limiting beam power is $P_l = 3.8\ kW$. Since P_l is relatively large compared to the thermal self-focusing thresholds, this calculation suggests that even though thermal self-focusing can greatly increase the beam intensity, it may be possible to maintain the beam power below the limiting value P_l thereby avoiding competition between DFWM and thermal self-focusing.

V. Conclusion

This paper has demonstrated that collisional effects may greatly enhance the PC reflectivity above the Steel and Lam result. The additional DFWM mechanism is predominantly the pressure gradient resulting from localized collisional heating. Using DDFWM, it may be possible to reduce the required pump power levels by taking advantage of a resonant frequency of the plasma. Numerical estimates of the PC reflectivity indicte that for modest power levels, gains of order unity are possible in the submillimeter to centimeter wavelength range without malevolent consequences from competing SRS, SBS, and self-focusing. These encouraging results suggest that a plasma is a viable PC medium in the infrared to centimeter wavelength range.

ACKNOWLEDGMENTS

The authors acknowledge the support of the Princeton Plasma Physics Laboratory under US DOE contract No. DE-AC02-76CHO3073. Helpful suggestions and guidance by E. Valeo, C. Oberman, and D. Meade are gratefully acknowledged.

One of the authors (J. F. Federici) is supported by a National Science Foundation Graduate Fellowship and by a Garden State Graduate Fellowship.

This research was funded by the Office of Innovative Science and Technology.

Appendix A.

The effective collision frequency is derived using the high frequency conductivity.[10]

$$\sigma_1 \simeq \frac{\omega_{pe}^2}{4\pi i\omega}([1 - \frac{(2\pi)^{\frac{1}{2}}e^2\omega_{pe}^2}{6m_e\omega v_{te}^3}] - i(\frac{2}{\pi})^{\frac{1}{2}}\frac{e^2\omega_{pe}^2}{6m_e\omega v_{te}^3}[\ln(\frac{2k_{max}v_{te}^2}{\omega^2}) - \gamma])^{-1} \quad \text{(A1)}$$

$$k^2c^2 = \omega^2(1 - \frac{4\pi i\sigma_1}{\omega}) \quad \text{(A2)}$$

The real part of Eq. (A2) yields the ordinary wave dispersion relation $\omega^2 = \omega_{pe}^2 + k_r^2c^2$. The imaginary portion determines the high frequency collision rate and attenuation coefficient.

$$\alpha = \frac{\omega_{pe}^2\nu_{hf}}{2\omega^2 c}(1 - \frac{\omega_{pe}^2}{\omega^2})^{-\frac{1}{2}} \quad \text{(A3)}$$

$$\nu_{hf} = \frac{\nu_e}{2}(1 + \frac{\ln(\sqrt{2}\frac{\omega_{pe}}{\omega}) - \frac{\gamma}{2}}{\ln\Lambda}) \quad \text{(A4)}$$

In the above equations, γ is Euler's constant and $\ln\Lambda$ is the coulomb logarithm.

References

[1]A. Yariv, J. Quant. Elect. **QE-14**, 650 (1978).

[2]D. M. Pepper, Opt. Eng. **21**, 156 (1982).

[3]V. V. Shkunov and B. Y. Zel'dovich, Sci. Amer., December (1985).

[4]D. M. Pepper, Sci. Amer., January (1986).

[5]D. Steel and J. Lam, Opt. Lett. **4**, 363 (1979).

[6]Q. Zhong, Chin. Phys. **2**, 141 (1982).

[7]R. A. Fisher, *Optical Phase Conjugation* (Academic Press, NY, 1985).

[8]G. Martin and R. W. Hellwarth, Appl. Phys. Lett. **34**, 371 (1979).

[9]I. B. Bernstein, C. E. Max, and J. J. Thomson, Phys. Fluids **21**, 905 (1978).

[10]J. Dawson and C. Oberman, Phys. Fluids **5**, 517 (1962); J. Dawson and C. Oberman, Phys. Fluids **6**, 394 (1963).

[11]J. AuYeung, D. Fekete, D. M. Pepper, A. Yariv, Opt. Lett. **4**, 42 (1979).

[12]C. E. Max, Phys. Fluids **19**, 74 (1976).

[13]W. Kruer, Comm. Plasma Phys. Contr. Fusion **9**, 63 (1985).

[14]D. W. Forslund, J. M. Kindel, and E. L. Lindman, Phys. Fluids **18**, 1002 (1975).

[15]J. F. Drake, P. K. Kaw, Y. C. Lee, G. Schmidt, C. S. Liu, and M. N. Rosenbluth, Phys. Fluids **17**, 778 (1974).

Figures

FIG. 1. Degenerate four-wave mixing geometry. The subscripts f, b, p, s refer to the foward pump, backward pump, probe, and signal wave, respectively.

FIG. 2. Phase conjugate reflectivity for a CW CO_2 laser with $\lambda = 10.6\ \mu m$, intensity $I = 200\ kW/cm^2$, interaction length $L = 5\ cm$. The upper curve is for $T_e = 0.75\ eV$. The lower curve corresponds to 1 eV. At $T_e = 0.75\ eV$ and $n_e \sim 2 \times 10^{16}\ cm^{-3}, k_{bp}\lambda_{mfp} \sim 1$. Straight lines indicate the Steel and Lam result.

FIG. 3. Phase conjugate reflectivity for pulsed CO_2 laser with $\lambda = 10.6\ \mu m$, intensity $I = 150\ MW/cm^2$, interaction length $L = 5\ cm$ at $T_e = 0.75$ and 1 eV. At $T_e = 0.75\ eV$ and $n_e \sim 2 \times 10^{16}\ cm^{-3}, k_{bp}\lambda_{mfp} \sim 1$.

FIG. 4. Reflectivity for far-infrared source with $\lambda = 119\ \mu m$, intensity $I = 2.5\ MW/cm^2$, interaction length $L = 2\ cm$, at $T_e = 0.75$ and 1 eV. At $T_e = 0.75\ eV$ and $n_e \sim 9 \times 10^{14}\ cm^{-3}, k_{bp}\lambda_{mfp} \sim 1$.

FIG. 5. Reflectivity for millimeter source with $\lambda = 2\ mm$, intensity $I = 20\ kW/cm^2$, interaction length $L = 5\ cm$, at $T_e = 0.75$ and 1 eV. At $T_e = 0.75\ eV$ and $n_e \sim 4 \times 10^{13}\ cm^{-3}, k_{bp}\lambda_{mfp} \sim 1$. Near cutoff large reflectivities are expected.

FIG. 6. Reflectivity for centimeter waves with $\lambda = 1\ cm$, intensity $I = 1\ kW/cm^2$, interaction length $L = 20\ cm$. Although the fluid equations are not valid, Steel and Lam's theory should give a reasonable result for 0.75 and 1 eV.

FIG. 7. DDFWM phase conjugate reflectivity for CW CO_2 laser with $\lambda = 10.6\ \mu m$, intensity $I = 200\ kW/cm^2$, interaction length $L = 5\ cm$ at the sound resonance (solid curve) and off resonance (dash).

FIG. 8. DDFWM reflectivity for far-infrared source with $\lambda = 119\ \mu m$, intensity $I = 50\ kW/cm^2$, interaction length $L = 2\ cm$ at the sound resonance (solid) and off resonance (dash).

FIG. 9. DDFWM reflectivity for millimeter source with $\lambda = 2\ mm$, intensity $I = 25\ W/cm^2$, interaction length $L = 5\ cm$ at the sound resonance (solid) and off resonance (dash). Near cutoff, the resonance increases the phase conjugate reflectivity by over three orders of magnitude.

86X0315

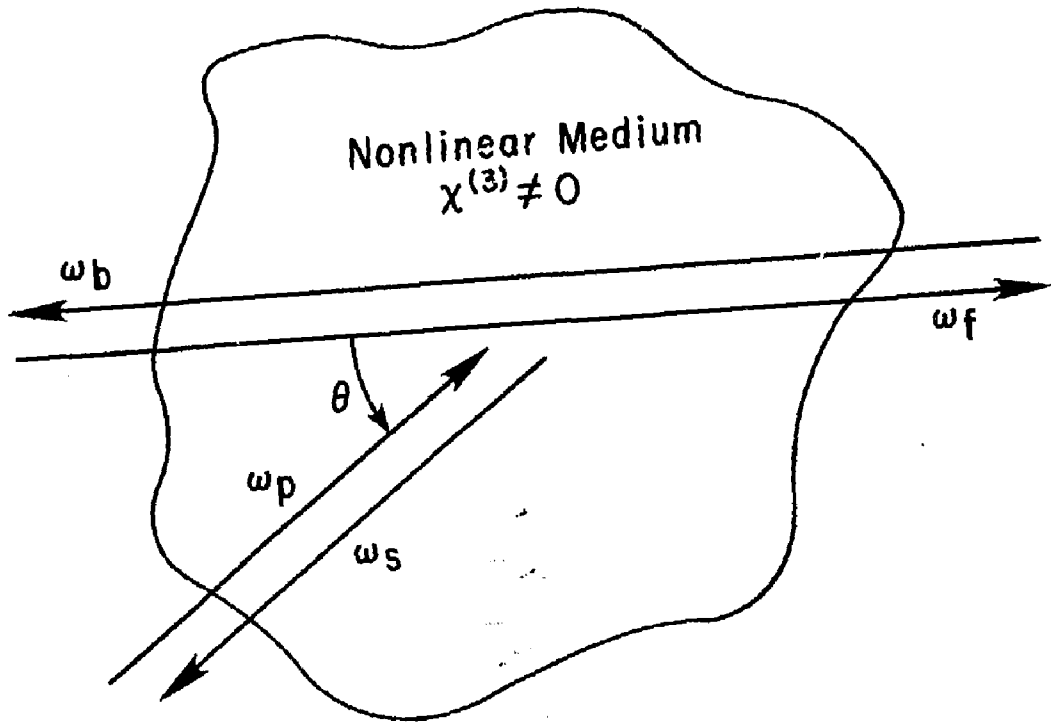

Fig. 1

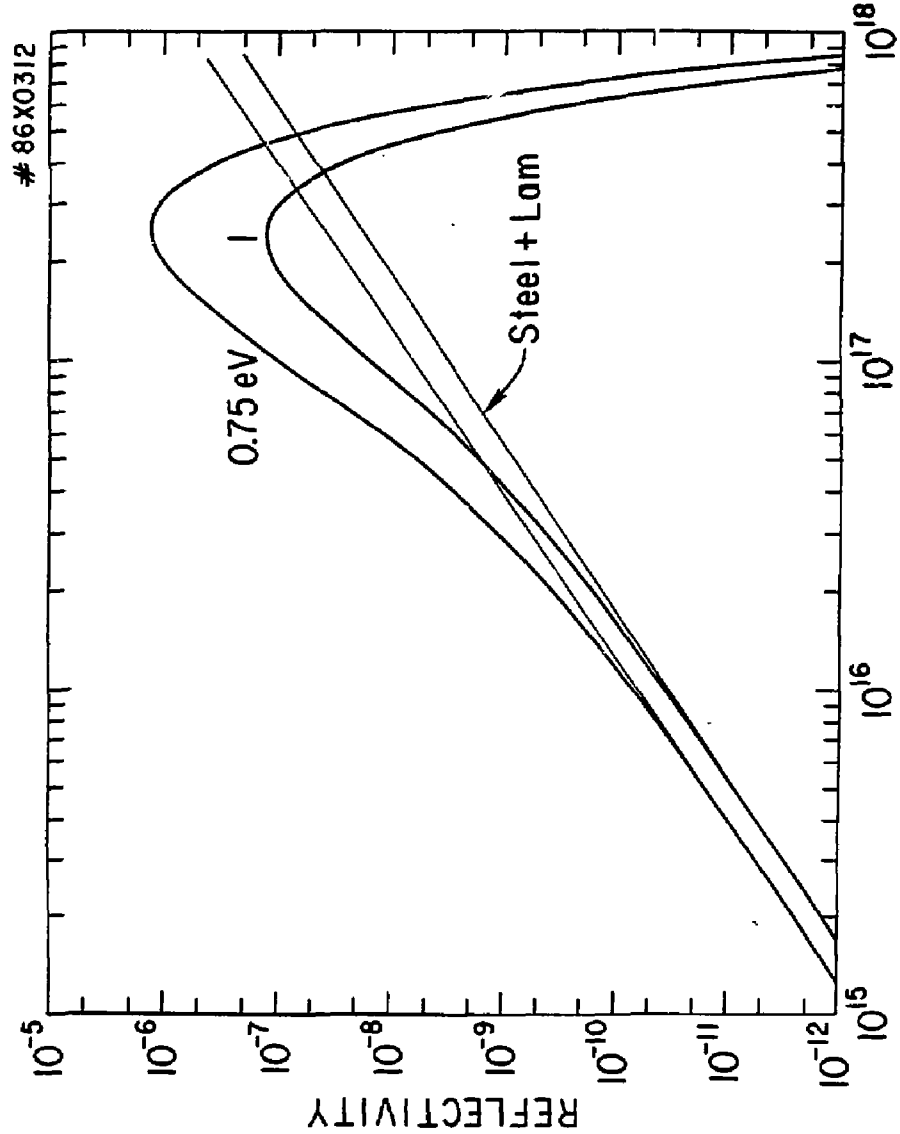
#86X0312
0.75 eV
I
Steel + Lam
REFLECTIVITY
ELECTRON DENSITY (cm^{-3})
10^{-5}
10^{-6}
10^{-7}
10^{-8}
10^{-9}
10^{-10}
10^{-11}
10^{-12}
10^{15}
10^{16}
10^{17}
10^{18}

Fig. 2

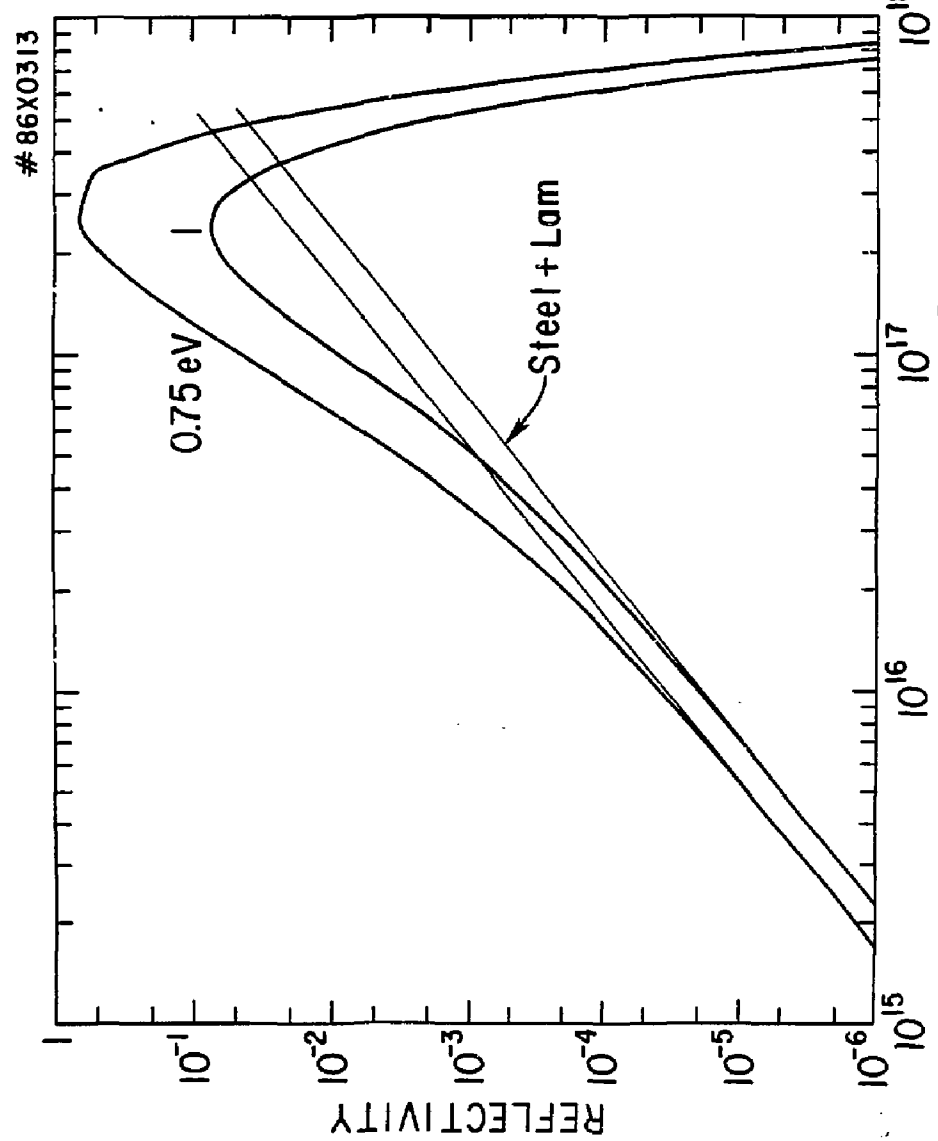
#86X0313
1
0.75 eV
Steel + Lam
REFLECTIVITY
1
10^{-1}
10^{-2}
10^{-3}
10^{-4}
10^{-5}
10^{-6}
10^{15}
10^{16}
10^{17}
10^{18}
ELECTRON DENSITY (cm^{-3})

Fig. 3

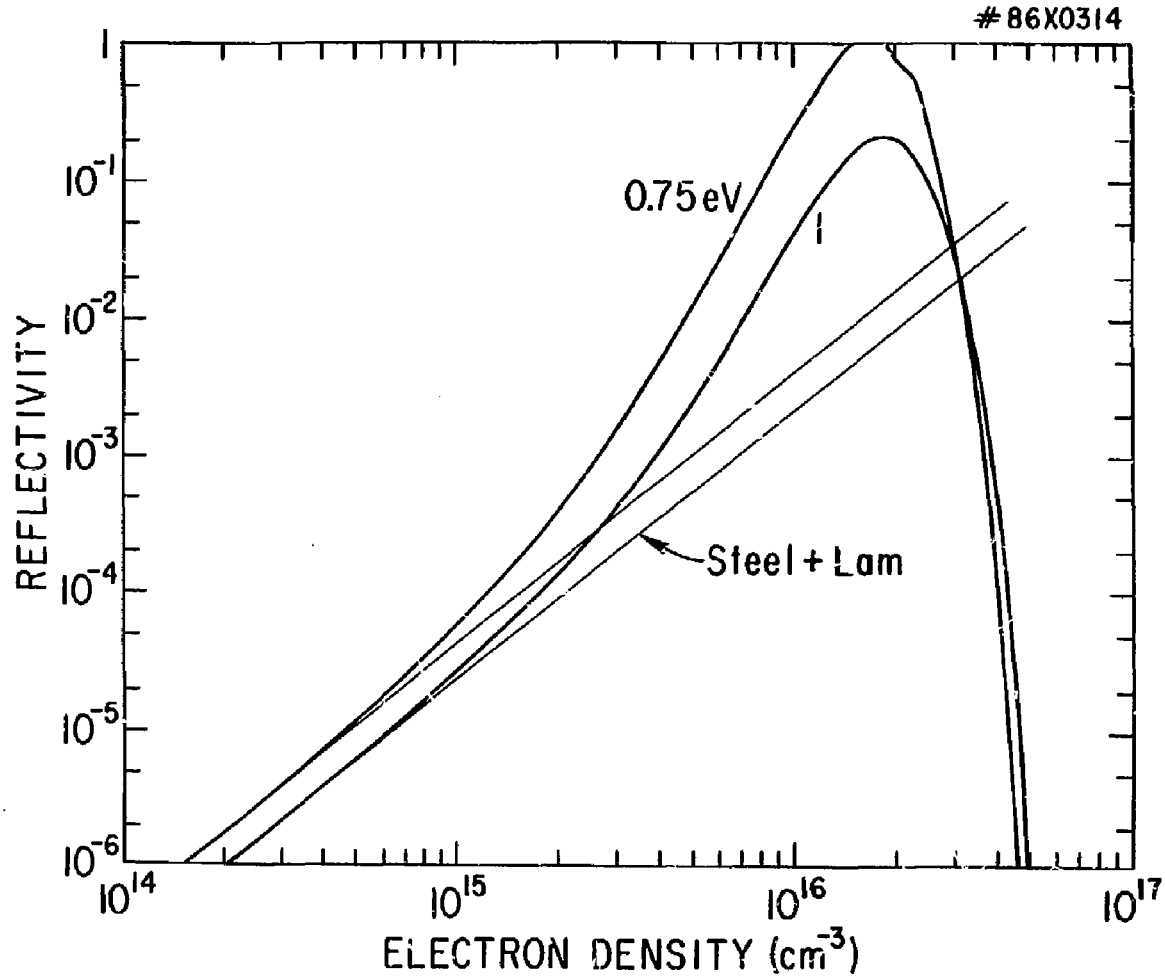
#86X0314
1
10^{-1}
10^{-2}
10^{-3}
10^{-4}
10^{-5}
10^{-6}
REFLECTIVITY
0.75 eV
1
Steel + Lam
10^{14}
10^{15}
10^{16}
10^{17}
ELECTRON DENSITY (cm^{-3})

Fig. 4

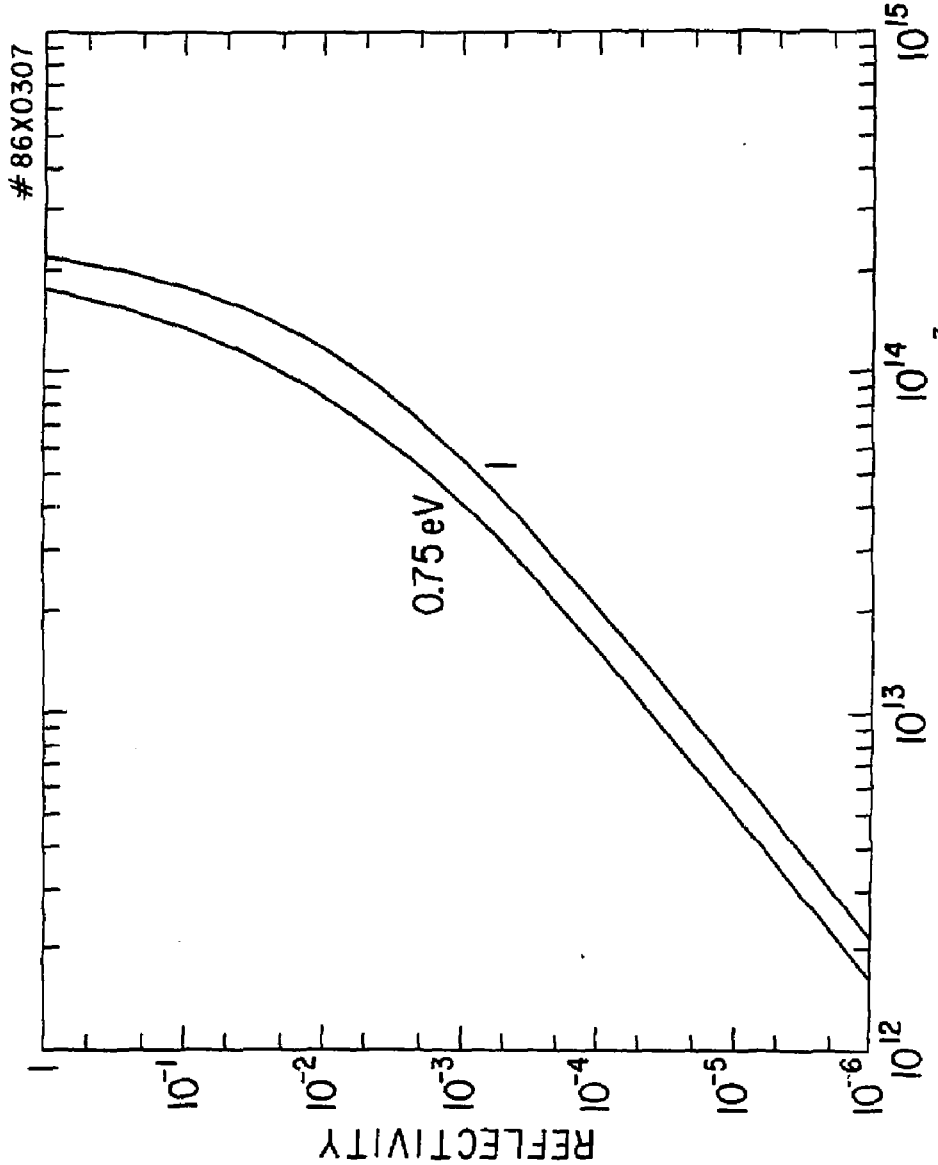
#86X0307
REFLECTIVITY
1
10^{-1}
10^{-2}
10^{-3}
10^{-4}
10^{-5}
10^{-6}
0.75 eV
1
10^{12}
10^{13}
10^{14}
10^{15}
ELECTRON DENSITY (cm^{-3})

Fig. 5

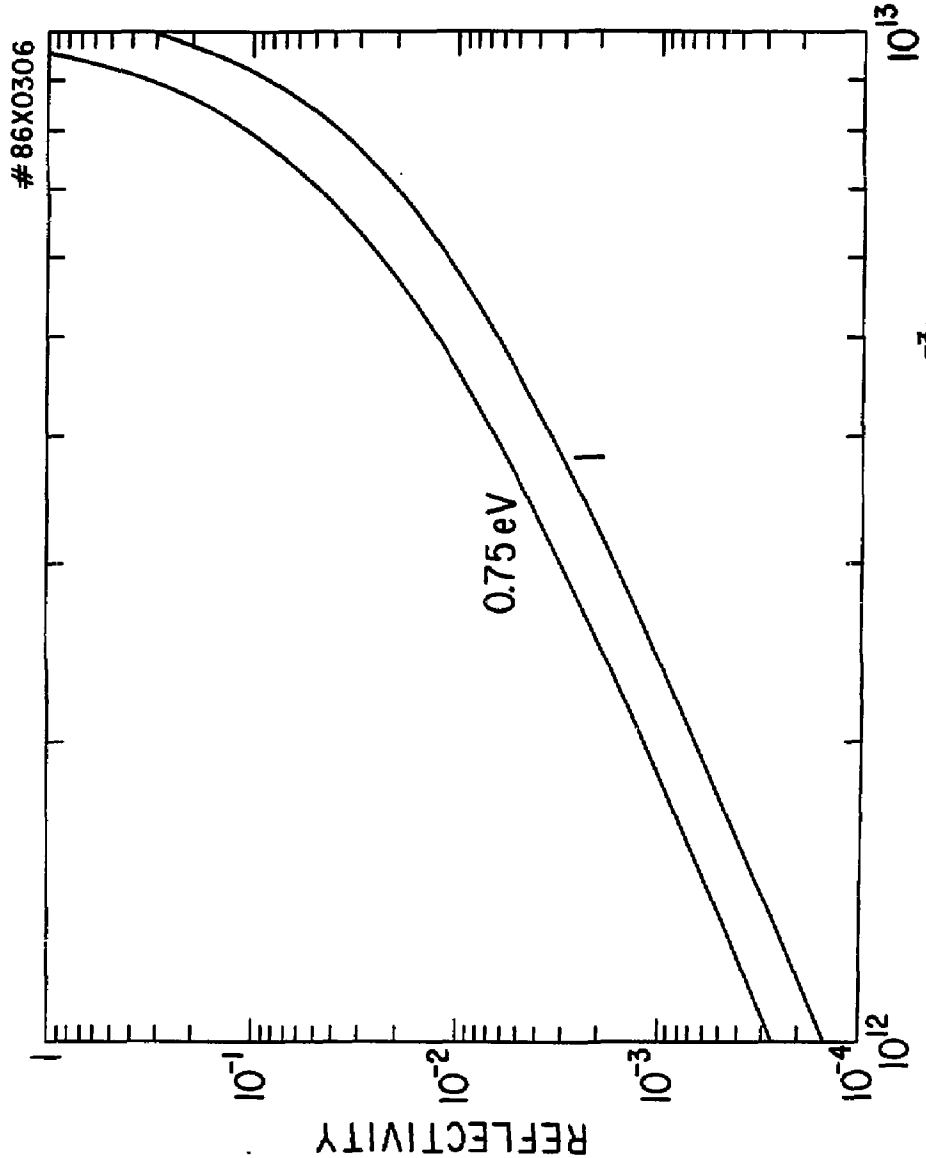
#86X0306
1
0.75 eV
REFLECTIVITY
1
10^{-1}
10^{-2}
10^{-3}
10^{-4}
10^{12}
10^{13}
ELECTRON DENSITY (cm^{-3})

Fig. 6

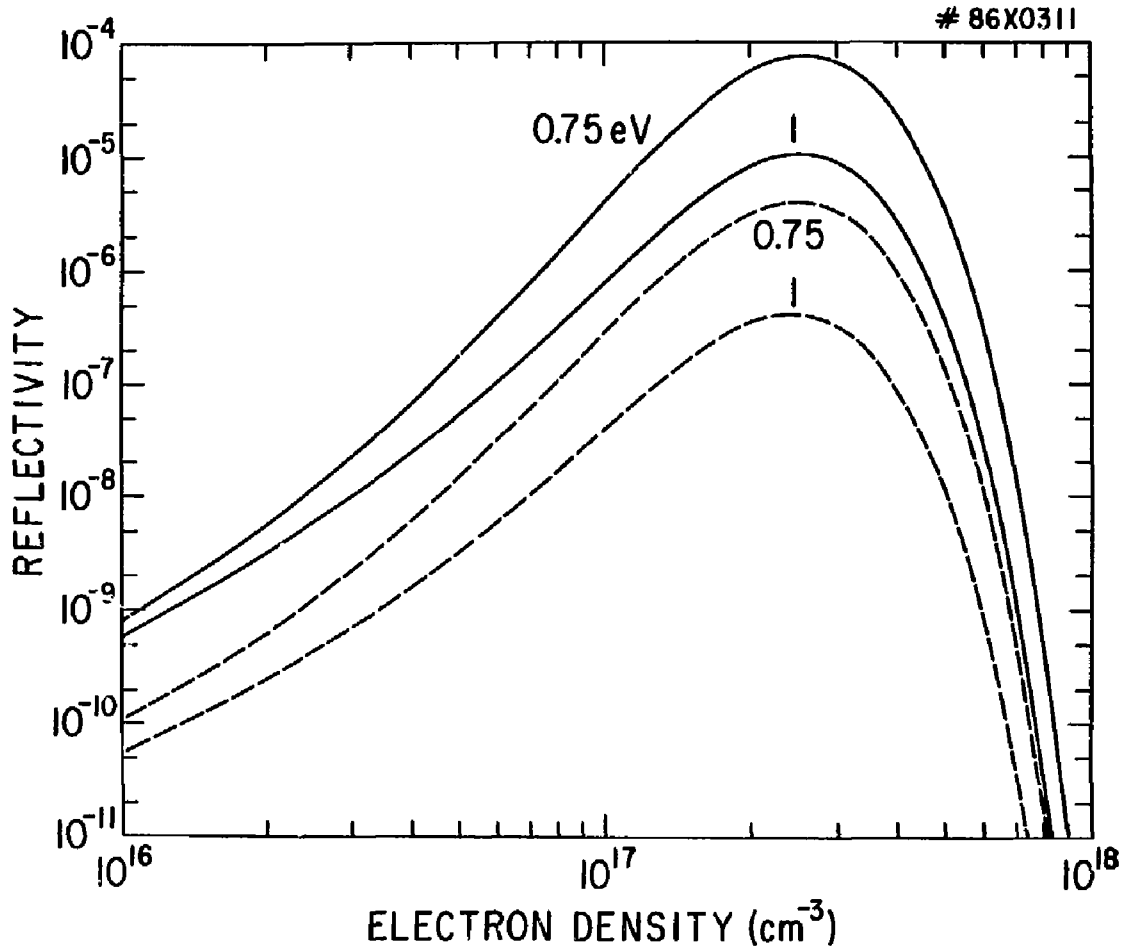
86X0311
0.75 eV
1
0.75
1
REFLECTIVITY
10^{-4}
10^{-5}
10^{-6}
10^{-7}
10^{-8}
10^{-9}
10^{-10}
10^{-11}
10^{16}
10^{17}
10^{18}
ELECTRON DENSITY (cm^{-3})

Fig. 7

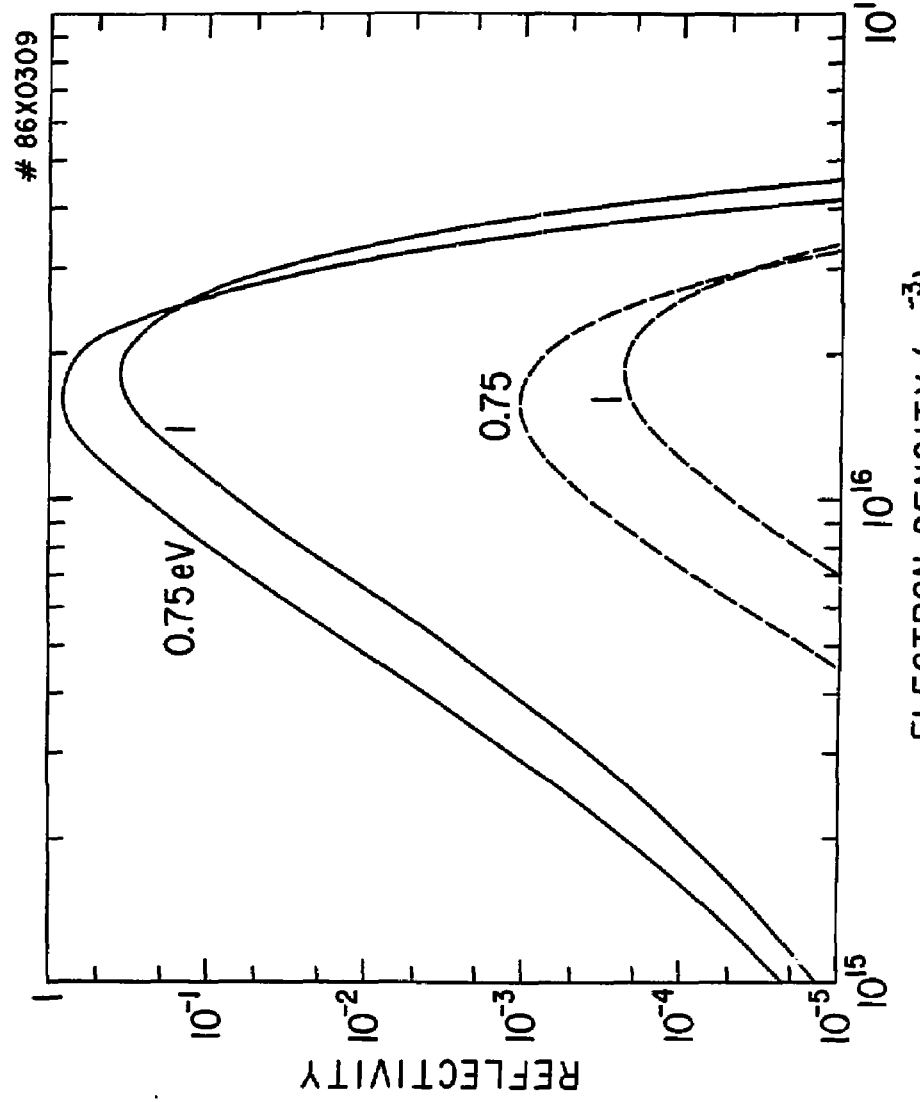
#86X0309
REFLECTIVITY
1
10^{-1}
10^{-2}
10^{-3}
10^{-4}
10^{-5}
0.75 eV
1
0.75
1
10^{15}
10^{16}
10^{17}
ELECTRON DENSITY (cm^{-3})

Fig. 8

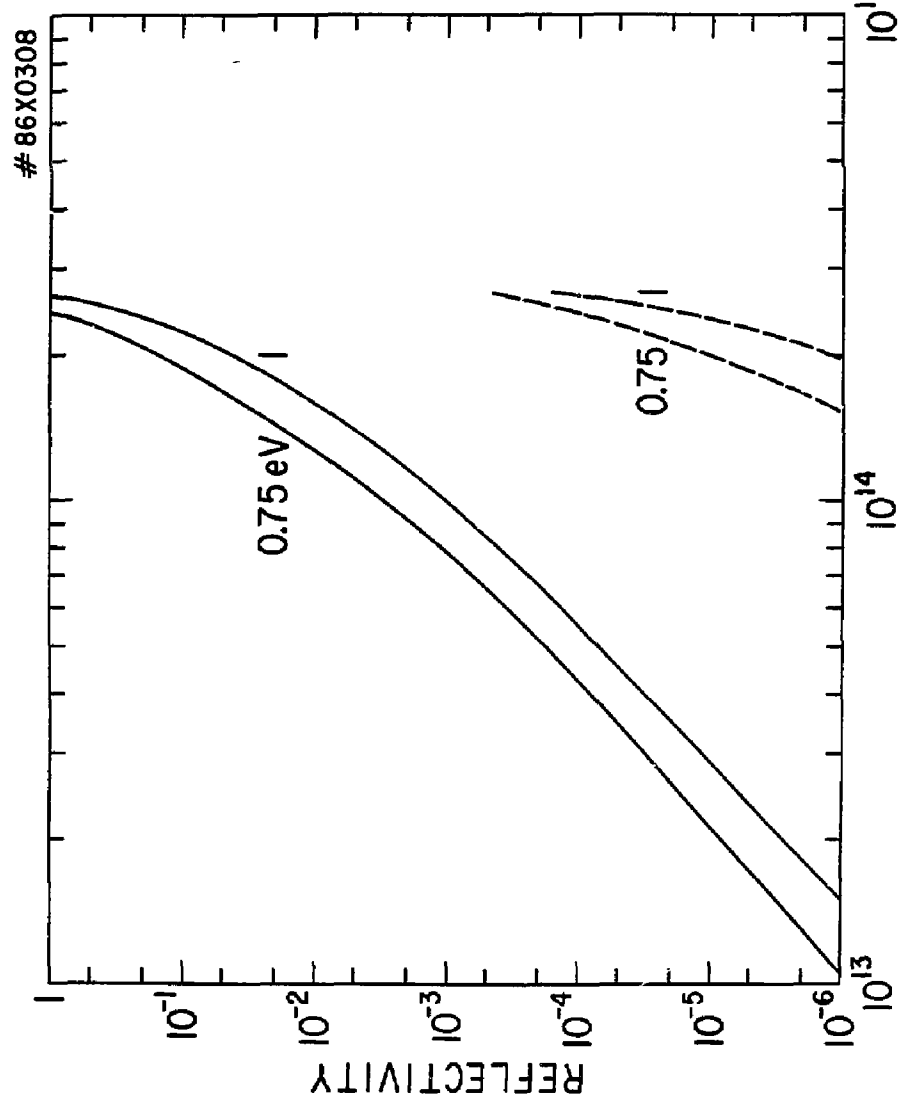
#86X0308
REFLECTIVITY
1
10^{-1}
10^{-2}
10^{-3}
10^{-4}
10^{-5}
10^{-6}
10^{13}
10^{14}
10^{15}
ELECTRON DENSITY (cm^{-3})
0.75 eV
1
0.75
1

Fig. 9

EXTERNAL DISTRIBUTION IN ADDITION TO UC-20

Plasma Res Lab, Austra Nat'l Univ, AUSTRALIA
Dr. Frank J. Paoloni, Univ of Wollongong, AUSTRALIA
Prof. I.R. Jones, Flinders Univ., AUSTRALIA
Prof. M.H. Brennan, Univ Sydney, AUSTRALIA
Prof. F. Cap, Inst Theo Phys, AUSTRIA
M. Goossens, Astronomisch Instituut, BELGIUM
Prof. R. Boucique, Laboratorium voor Natuurkunde, BELGIUM
Dr. D. Palumbo, Dg XII Fusion Prog, BELGIUM
Ecole Royale Militaire, Lab de Phys Plasmas, BELGIUM
Dr. P.H. Sakanaka, Univ Estadual, BRAZIL
Lib. & Doc. Div., Instituto de Pesquises Espaciais, BRAZIL
Dr. C.R. James, Univ of Alberta, CANADA
Prof. J. Teichmann, Univ of Montreal, CANADA
Dr. H.M. Skarsgard, Univ of Saskatchewan, CANADA
Prof. S.R. Sreenivasan, University of Calgary, CANADA
Prof. Tudor W. Johnston, INRS-Energie, CANADA
Dr. Hannes Barnard, Univ British Columbia, CANADA
Dr. M.P. Bachynski, MPB Technologies, Inc., CANADA
Chalk River, Nucl Lab, CANADA
Zhengwu Li, SW Inst Physics, CHINA
Library, Tsing Hua University, CHINA
Librarian, Institute of Physics, CHINA
Inst Plasma Phys, Academia Sinica, CHINA
Dr. Peter Lukac, Komenskeho Univ, CZECHOSLOVAKIA
The Librarian, Culham Laboratory, ENGLAND
Prof. Schatzman, Observatoire de Nice, FRANCE
J. Radet, CEN-BP6, FRANCE
JET Reading Room, JET Joint Undertaking, ENGLAND
AM Dupas Library, AM Dupas Library, FRANCE
Dr. Tom Must, Academy Bibliographic, HONG KONG
Preprint Library, Cent Res Inst Phys, HUNGARY
Dr. R.K. Chhajlani, Vikram Univ, INDIA
Dr. B. Dasgupta, Saha Inst, INDIA
Dr. P. Kaw, Physical Research Lab, INDIA
Dr. Phillip Rosenau, Israel Inst Tech, ISRAEL
Prof. S. Cuperman, Tel Aviv University, ISRAEL
Prof. G. Rostagni, Univ Di Padova, ITALY
Librarian, Int'l Ctr Theo Phys, ITALY
Miss Clelia De Palo, Assoc EURATOM-ENEA, ITALY
Biblioteca, del CNR EURATOM, ITALY
Dr. H. Yamato, Toshiba Res & Dev, JAPAN
Direc. Dept. Lg. Tokamak Dev. JAERI, JAPAN
Prof. Nobuyuki Inoue, University of Tokyo, JAPAN
Research Info Center, Nagoya University, JAPAN
Prof. Kyoji Nishikawa, Univ of Hiroshima, JAPAN
Prof. Sigeru Mori, JAERI, JAPAN
Prof. S. Tanaka, Kyoto University, JAPAN
Library, Kyoto University, JAPAN
Prof. Ichiro Kawakami, Nihon Univ, JAPAN
Prof. Satoshi Itoh, Kyushu University, JAPAN
Dr. D.I. Choi, Adv. Inst Sci & Tech, KOREA
Tech Info Division, KAERI, KOREA
Bibliotheek, Fom-Inst Voor Plasma, NETHERLANDS
Prof. B.S. Liley, University of Waikato, NEW ZEALAND
Prof. J.A.C. Cabral, Inst Superior Tecn, PORTUGAL
Dr. Octavian Petrus, ALI CUZA University, ROMANIA
Prof. M.A. Hellberg, University of Natal, SO AFRICA
Dr. Johan de Villiers, Plasma Physics, Nucor, SO AFRICA
Fusion Div. Library, JEN, SPAIN
Prof. Hans Wilhelmson, Chalmers Univ Tech, SWEDEN
Dr. Lennart Stenflo, University of UMEA, SWEDEN
Library, Royal Inst Tech, SWEDEN
Centre de Recherchesen, Ecole Polytech Fed, SWITZERLAND
Dr. V.T. Tolok, Kharkov Phys Tech Ins, USSR
Dr. D.D. Ryutov, Siberian Acad Sci, USSR
Dr. G.A. Eliseev, Kurchatov Institute, USSR
Dr. V.A. Glukhikh, Inst Electro-Physical, USSR
Institute Gen. Physics, USSR
Prof. T.J.M. Boyd, Univ College N Wales, WALES
Dr. K. Schindler, Ruhr Universitat, W. GERMANY
ASDEX Reading Rm, IPP/Max-Planck-Institut fur Plasmaphysik, F.R.G.
Nuclear Res Estab, Julich Ltd, W. GERMANY
Librarian, Max-Planck Institut, W. GERMANY
Bibliothek, Inst Plasmaforschung, W. GERMANY
Prof. R.K. Janev, Inst Phys, YUGOSLAVIA